Carbohydrate Polymers 157 (2017) 48–56

Contents lists available at ScienceDirect

Carbohydrate Polymers

journal homepage: www.elsevier.com/locate/carbpol

Synthesis and swelling behaviors of carboxymethyl cellulose-based superabsorbent resin hybridized with graphene oxide

Zhimin Wang[a,*], Aimin Ning[a], Puhui Xie[a], Guangqin Gao[a], Lixia Xie[a], Xin Li[a], Andong Song[b,*]

[a] School of Science, Henan Agricultural University, Zhengzhou 450002, P.R. China
[b] College of Life Science, Henan Agricultural University, Zhengzhou 450002, P.R. China

ARTICLE INFO

Article history:
Received 31 July 2016
Received in revised form 7 September 2016
Accepted 22 September 2016
Available online 23 September 2016

Keywords:
Carboxymethyl cellulose
Superabsorbent resin
Graphene oxide
Swelling behavior
Water retention

ABSTRACT

Well-dispersed graphene oxide sheets were successfully incorporated into a superabsorbent resin through *in situ* graft polymerization of acrylic acid on carboxymethyl cellulose backbone in the presence of graphene oxide as filler. The structure and properties of the resultant superabsorbent resin were studied in detail by means of a variety of characterization methods. The influence of the feed ratio of starting materials (such as GO, initiator, cross-linker, the ratio of CMC to AA and the neutralized degree of AA) and pH values on water absorbency and retention ability was extensively determined and discussed. The obtained results showed that the introduction of graphene oxide had no obvious influence on the inherent structure of the superabsorbent resin but changed the surface morphology significantly. Importantly, the hybrid superabsorbent resin showed an enhanced thermal stability and remarkably improved swelling ratio as well as water-retention ability comparing with that of the pure superabsorbent resin.

1. Introduction

Superabsorbent resin (SAR) represents a new type of functional hydrogel with an appropriate degree of cross-linking and polymer network structure. SAR can absorb large volumes of water or aqueous solutions in a relatively short time and retain swollen state even under certain pressure (Ma, Li et al., 2015; Mukerabigwi et al., 2016). Because of these excellent characteristics, SARs are extensively used in many fields, such as agriculture, horticulture, hygienic products, wastewater treatment, drug delivery and coal dewatering, and so on. Generally, raw materials for preparing commercial SARs have almost focused on petrochemical products, such as acrylic acid, acrylamide, polyvinyl alcohol, and acrylonitrile. Though the SARs produced from synthetic polymers with superior price-to-efficiency balance, high production cost and serious environmental problem have been two major concerns for these SARs (Ma, Ran et al., 2015; Mukerabigwi et al., 2015). In this regard, the development of eco-friendly natural-based SARs with low production cost and good biodegradability will be highly desired.

To date, various alternatives and strategies have been proposed to prepare low cost and eco-friendly SARs (Bao, Ma, & Sun, 2012; Chen, Zhang, & Li, 2015; Liu, Li et al., 2013; Muhammad et al., 2016). Among them, copolymerization of natural polysaccharides such as starch, cellulose or chitosan with hydrophilic synthetic polymers have been proved to be a popular and applicable method. Nevertheless, the lower swelling ratio and weaker gel strength of these SARs relative to the petro-based products severely restrict their practical application (Bao et al., 2012; Liu, Li et al., 2013; Muhammad et al., 2016; Mukerabigwi et al., 2016; Wang & Wang, 2010). To this end, much effort has been made on developing economic and more effective polysaccharide based hydrogels through different strategies, and much progress has been achieved during past few years (Huang, Liu, Fang, & Zhang, 2013; Ma, Li et al., 2015; Mukerabigwi et al., 2016; Peng et al., 2016). Among them, hybridizing inorganic nanomaterials with SARs have attracted more and more interest owing to their synergistic properties and potential applications in various fields. The incorporation of these nano-fillers can not only reduce production cost, but also improve swelling ability, gel strength, and thermal stability of the corresponding SARs. To date, different additives, such as montmorillonite, kaolin, attapulgite, and vermiculite have been used to fabricate hybrid SARs (Bao, Ma, & Li, 2011; Bao et al., 2012; Zhu et al., 2012).

* Corresponding authors.
E-mail addresses: gary1451@iccas.ac.cn (Z. Wang), song1666@126.com (A. Song).

http://dx.doi.org/10.1016/j.carbpol.2016.09.070
0144-8617/

Ever since Novoselov et al. succeeded in extracting single atom-thick layer from bulk graphite in 2004 (Novoselov et al., 2004), graphene oxide (GO) and graphene have attracted considerable attention for use in numerous applications including nanocomposites due to their unique structural and fascinating properties (Wang, Xu, Gao, & Li, 2014). GO consists of a considerable number of covalently attached oxygen-containing groups such as hydroxyl, epoxy, carbonyl and carboxyl groups. The existence of these groups makes GO sheets good hydrophilicity and the ability to be well dispersed in aqueous media by mild ultrasonic treatment (Compton & Nguyen, 2010). Though a few investigations devoted to GO-based composite hydrogels (Liu et al., 2016; Zhang, Zhai, & He, 2014), very few reports were on GO-based SARs until now (Huang et al., 2012; Liu, Yu et al., 2013; Morimune, Nishino, & Goto, 2012; Zhu et al., 2012). Besides, the raw materials concerned in these documents are almost based upon petrochemical products. There are few literatures using biodegradable natural polysaccharides as raw materials for preparing GO-based SAR (Huang et al., 2016). It is expected that a new type of SAR with novel structure and improved performance can be developed by the effective combination of biodegradable natural polysaccharide and GO.

In the present study, GO sheets were successfully incorporated into a carboxymethyl cellulose (CMC)-based SAR by grafting polymerization of partially neutralized acrylic acid (AA) onto CMC backbones in the presence of GO as fillers. The inherent structure and surface morphology of the hybrid SAR (HSAR) were compared with that of the pure SAR. The effects of the feed ratio of starting materials (such as GO, initiator, cross-linker, the ratio of CMC to AA and the neutralized degree of AA) and pH values on the swelling behavior of the HSARs were systematically investigated. The effect of GO on the water retention abilities of the prepared HSAR in distilled water at different temperature were also examined.

2. Experimental

2.1. Materials

AA (A.R.), Ammonium persulfate (APS, A.R.), CMC (C.R., 300–800 mPa s) and *N,N*-methylene bisacrylamide (MBA, C.R.) were purchased from Sinopharm Chemical Reagent Co., Ltd, China. AA was distilled under reduced pressure before use. All the reagents used in this study were of reagent grade. All other reagents were used as received and all solutions were prepared with distilled water.

2.2. Preparation of CMC-g-PAA/GO HSAR

The graphite oxide was synthesized from natural graphite powder by the modified Hummers method as originally presented by Kovtyukhova and colleagues (Hummers & Offeman, 1958; Kovtyukhova et al., 1999). The obtained graphite oxide was dispersed in deionized water and subsequently sonicated to yield exfoliated GO. A typical procedure for CMC-*g*-PAA/GO HSAR was performed as follows: CMC powder (5–20 wt% of AA) was dissolved in 30 mL distilled water in a 250 mL four-necked flask equipped with a mechanical stirrer, a thermometer, a reflux condenser and a nitrogen line to form a transparent sticky solution. The solution was heated to 60 °C and purged with N_2 for 30 min to remove dissolved oxygen. Then, 5 mL of APS aqueous solution with adequate amount was added under continuous stirring and kept at 60 °C for 10 min to generate radicals. AA (7.2 g) with various neutralization degree from 40 to 90%, MBA cross-linker (0.01–0.1 wt% of AA) and the calculated amount of GO powder for different final contents (0; 0.1 wt%; 0.3 wt%; 0.5 wt%; 0.8%; 1.0 wt%) were stirred or sonicated for 1 h until the mixture was dissolved completely. After cooling to 50 °C, the mixture was added to the flask. The temperature was risen to 70 °C and maintained for 3 h to complete reaction. A nitrogen atmosphere was maintained throughout the reaction period. The obtained hydrogel products were washed with distilled water for several times and dried to constant weight at 70 °C. Finally, the dried HSAR was ground and sieved to 80 meshes for further use.

2.3. Materials characterization

The synthesis of GO and HSARs were characterized comprehensively by a variety of techniques. The X-ray photoelectron spectroscopy (XPS) data were obtained with VG Multilab 2000 electron spectrometer from Thermo Scientific using 300 W Al Kα radiations. The base pressure was about 3×10^{-9} mbar. The binding energies were referenced to the C1s line at 284.8 eV from adventitious carbon. Wide angle X-ray diffraction (WXRD) measurements were made using a Bruker D8 ADVANCE X-ray diffractometer with Cu Ka (1.541 Å) radiation (40 kV, 30 mA). Powder samples were mounted on a sample holder and scanned with a step size of 0.01° in the angular region between 2θ = 3° and 90°. AFM image was taken by using a Multimode 8 microscope (Bruke Veeco, Inc.) operating in the tapping mode with standard silicon nitride tips. Typically, the surface was scanned at 1 Hz with the resolution of 256 lines/image. For scanning electron microscopy (SEM) observations, the specimens were dropped onto the silicon single crystal sheet and dried under infrared light. The dried specimens were placed carefully on conducting glue, then coated with gold vapor to make them conducting and analyzed on a JSM 6700F SEM operated at 5.0 kV. The thermal stabilities were determined using a NETZSCH4 TGA instrument at a 50 mL min^{-1} flow rate under a nitrogen atmosphere. The temperature was increased from 50 to 800 °C at a rate of 10 °C min^{-1}. The FT-IR spectra were obtained using a Nicolet Avator 230 spectrometer. The samples were prepared with KBr.

2.4. Swelling behaviors

The pre-weighted dry SAR was immersed in excessive distilled water and kept undisturbed for 10 h at room temperature until equilibrium swelling was reached. The swollen superabsorbent was filtered using a 100-mesh sieve and drained for 20 min until no free water remained. After weighing the swollen SAR, the equilibrium water absorption can be calculated by using the following equation.

$$Q_{eq} = (w_2 - w_1)/w_1 \quad (1)$$

where Q_{eq} is the equilibrium water absorption defined as grams of water per gram of sample; w_1 and w_2 are the mass of sample before and after swelling, respectively. All of the data were given as means ± SD (n = 3).

2.5. Water retention properties

Water retention behaviors of the optimal HSAR with 0.6 wt% GO were measured and compared with pure SAR by two different methods, i.e. heating test and centrifuging test. For the heating test, the pre-weighted swollen HSAR (w_2) equilibrated in distilled water was put into beaker and placed into an oven with the temperature of 100 °C. The water retention study was measured as a function of time by weighing the sample at certain time intervals. The mass of HSAR were recorded and marked as w_3. For the centrifuging test, the pre-weighted swollen HSAR (w_2) samples were centrifuged at 4000 rpm for 10 min continuously each time. The water retention study was measured as a function of time by weighing the sample at certain time intervals. The mass of HSAR were recorded and marked as w_3. As a control, the water retention behaviors of the pure SAR were tested under the same condition.

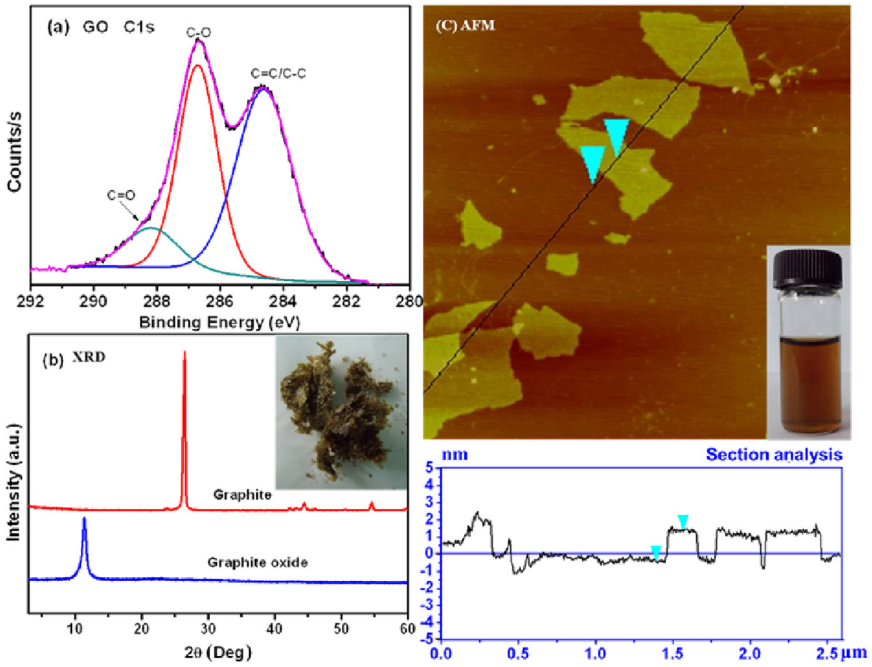

Fig. 1. a) C1s XPS spectrum of GO; b) X-ray diffraction profiles of graphite and GO, the inset is the photo of Lyophilized GO; c) AFM image and the height profile of GO, the inset shows the water dispersibility of GO.

The percentage of water retention is calculated as follows:

$$\text{Water retention } (\%) = (w_3/w_2) \times 100 \quad (2)$$

3. Results and discussion

3.1. Synthesis and characterization of GO

There are a wide range of oxygenic functional groups such as epoxy, hydroxyls, and carbonyl and ketone and carboxylic acid, both on the basal planes and at the edges of GO sheets. These hydrophilic groups facilitate GO exfoliated and dispersed readily in aqueous solution to produce homogeneous colloidal suspensions (Dreyer, Park, Bielawski, & Ruoff, 2010; Tripathi & Mitra, 2016). These properties are critical factors which will influence the properties of GO based composites, especially hydrogels or SARs. The chemical structure, morphology and dispersibility of the as-prepared GO were characterized by XPS, XRD and AFM measurements and shown in Fig. 1.

As shown in Fig. 1a, after oxidation of the graphite into GO, two dominant XPS peaks were observed at 284.7 and 286.8 eV. The peak at 284.7 eV is a characteristic peak for C=C/C—C bonding of graphite. The other peak at 286.8 eV shows a broad tail to higher binding energy region, which is attributed to emission from the oxidized carbon atoms in the GO. The three fitted peaks at 284.7, 286.8 and 287.9 eV can be assigned to the binding energies of carbon in C=C/C—C, C—O (epoxy/hydroxyls), and C=O (carbonyl/ketone), respectively, indicating the formation and existence of considerable amounts of oxygen containing groups on the surface of GO. This conclusion was further confirmed by the FT-IR spectroscopic measurement of GO (Fig. 2d).

The interlayer distances of both natural graphite and GO were investigated by XRD. As shown in Fig. 1b, a sharp diffraction peak near 26° was observed, implying an interlayer distance of 3.34 Å of the natural graphite. For the XRD pattern of GO, the diffraction peak near 26° disappeared while a new diffraction peak arose at 12°, which is the well-known peak position of GO, indicating that the natural graphite has been transferred into GO after oxidation.

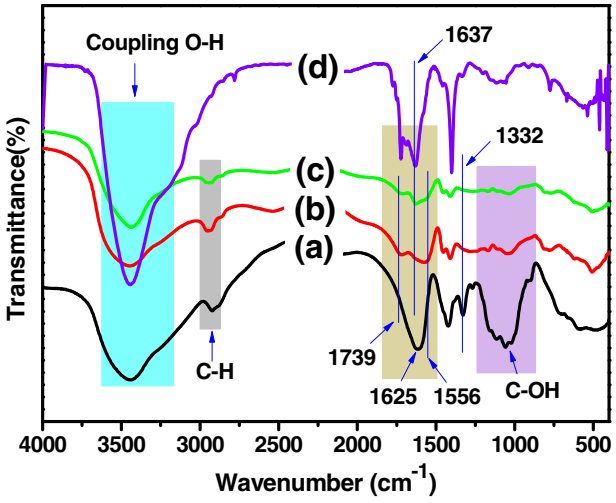

Fig. 2. The FT-IR spectra of (a) CMC, (b) CMC-*g*-PAA, (c) CMC-*g*-PAA/GO (0.6 wt% GO), and (d) GO.

The distances of the interlayers of GO were calculated to be 7.30 Å compared to that of 3.34 Å for natural graphite, in agreement with previous result (Wilson et al., 2009). This is also consistent with the fluffy appearance of the lyophilized GO (inset in Fig. 1b).

The AFM image of the GO sample (Fig. 1c), which were deposited onto a silica wafer from an aqueous dispersion, indicated that the thickness of the GO sheets averaged ca. 2 nm, indicating that the GO are in few-layered structures. Compared with natural graphite, the GO became strongly hydrophilic and could be dispersed in water forming a stable aqueous dispersion by mild ultrasonic treatment (Fig. 1c, inset).

3.2. Synthesis and characterization of HSARs

For investigation of the chemical structural changes from graft copolymerization to the formation of hybrid hydrogels, FT-IR

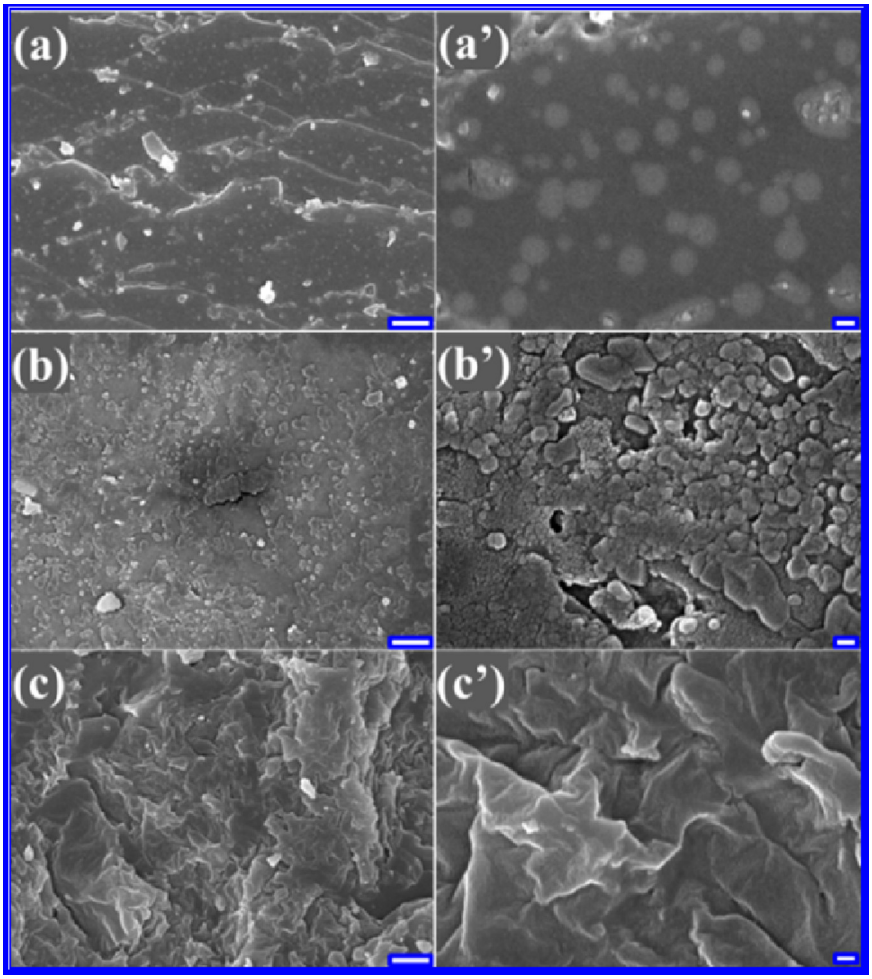

Fig. 3. SEM micrographs of (a and a') CMC-*g*-PAA, (b and b') CMC-*g*-PAA/GO (0.6 wt% GO) and (c and c') CMC-*g*-PAA/GO (1.0 wt% GO). The scale bars in left and right column represent 1 μm and 100 nm, respectively.

spectroscopic measurements of CMC, GO, CMC-*g*-PAA, and CMC-*g*-PAA/GO (0.6 wt%) were performed and displayed in Fig. 2. It can be seen that the characteristic absorption bands of CMC at 1061, 1115 and 1159 cm^{-1} (stretching vibrations of C—OH) were obviously weakened after copolymerization (Fig. 2a and b). Two new bands at 1739 cm^{-1} and 1556 cm^{-1} attributing to the C=O stretching of —COOH and asymmetric stretching of —COO— groups, appeared in the spectra of CMC-*g*-PAA and CMC-*g*-PAA/GO (Fig. 2b and c), indicating that PAA was grafted onto the CMC backbone. The asymmetric stretching vibration of C=O groups on CMC at 1625 cm^{-1} can be observed which overlapped with the characteristic absorption of —COO— groups of grafted PAA chains and formed a broad band. The —COO— bands of CMC-*g*-PAA at 1556 cm^{-1} almost disappeared after forming CMC-*g*-PAA/GO hybrid hydrogel, which implied the incorporation of GO decreased the bonding interaction between polymer chains compared to that of CMC-*g*-PAA hydrogel. In addition, The coupling O—H stretching vibration and the —OH bending vibration at 3550 cm^{-1} and 1480 cm^{-1} of GO weakened obviously in the spectrum of the hybrid hydrogel (Fig. 2c and d). Meanwhile, the characteristic absorption band of GO at 1637 cm^{-1} appeared in the spectrum of CMC-*g*-PAA/GO with a weakened intensity (Fig. 2c). All of these signals revealed that the GO sheets participated in the formation process of the HSAR through its surface active groups. A magnified FTIR plot for all samples in the range of 2000–800 cm^{-1} for more clarity of explanations was provided in the section of Supporting information (Fig. S1).

Since the GO sheets participated in the formation process of the hybrid SAR, it would be important to examine the possible effect of GO on the underlying structure of the SARs. To this end, the wide-angle X-ray diffractions were conducted to trace the alteration of the crystalline structure. However, as shown in Fig. S2, the patterns of the HSARs with different GO contents were nearly the same with that of the pure CMC-*g*-PAA SAR. This result indicates that the addition of GO had no effect on the formation mechanism of SAR. Nor is this all, the characteristic diffraction peak of GO at 12° does not appear in the XRD pattern of HSARs (Fig. S2b and c). This result might on the one hand because the feed ratio of GO was too little to be detected. But on the other hand, we thought more possible reason was that the majority of GO sheets have been exfoliated and dispersed uniformly into the SAR matrix which resulted the disappearance of the diffraction signal of GO. A similar effect of SWNTs on the α-CD based hybrid hydrogel was also reported in the literatures (Wang & Chen, 2007).

The effect of GO sheets on the thermal stability of the synthesized HSAR was also investigated using the TGA technique. Fig. S3 shows the thermograms of CMC-*g*-PAA, CMC-*g*-PAA/GO (0.6 wt%) and CMC-*g*-PAA/GO (1.0 wt%) in range of 50–800 °C. It was notable that three thermograms exhibited similar three-stage thermal decomposition processes after the earlier weight loss of 14.16% at 237 °C which was due to the loss of absorbed and bounded water. At the initial stage, three samples showed similar weight loss of about 21.72% between 237 and 405 °C which attributed to the dehydration of saccharide rings, the breaking of C—O—C bonds

in the chain of CMC and the elimination of the water molecule from the two neighboring carboxylic groups of the PAA chains due to the formation of anhydride and main-chain scission (Huang, Lu, & Xiao, 2007). In this stage, the introduction of GO sheets had almost no effect on the thermal decomposing process. The secondary decomposition stage occurred in the range of 401–475 °C for CMC-*g*-PAA, 404–487 °C for CMC-*g*-PAA/GO (0.6 wt%), and 409–499 °C for CMC-*g*-PAA/GO (1.0%) under the same weight loss of 17.65%. This stage should be attributed to the breakage of PAA chains and the destruction of cross-linked network structure network of SARs (Wang & Wang, 2010). Obviously, this process is delayed for the HSARs due to the introduction of GO sheets. With the increase of GO amounts from 0 to 1.0 wt%, the degradation temperature enhanced from 475 to 499 °C. This result further confirmed the cross-linking role of GO sheets. A detail description of the degradation process for three samples in this stage was provided in a tabulated form in the section of Supporting information (Table S1). Subsequently, the thirdly breakdown stage occurred with successive weight loss of about 15.82% until 600 °C for three hydrogel samples, this stage can be attributed to the destruction of carboxylic groups and CO_2 evolution, main chain scission and the breakage of the cross-linked network structure (Chen et al., 2015; Ma, Ran et al., 2015). Based on the abovementioned information, it can be concluded that the HSARs show lower weight loss rate and smaller total weight loss compared with pure SAR, which indicates that the incorporation of GO is helpful to improve the thermal stability of hydrogel. This result may contribute to the "tortuous path" effect which delays the permeation of oxygen and the escape of volatile degradation products. A similar effect on the thermal resistance of hydrogel composites was also reported in the literatures (Ferfera-Harrar, Aiouaz, Dairi, & Hadj-Hamou, 2014; Irani, Ismail, & Ahmad, 2014).

To examine the effect of GO sheets on the surface morphology of the resultant HSARs, SEM observation of CMC-*g*-PAA, CMC-*g*-PAA/GO (0.6 wt% GO) and CMC-*g*-PAA/GO (1.0 wt% GO) were conducted and their images with low (left column) and high magnification (right column) were presented in Fig. 3. It could be seen that the fracture surface morphology of the pure hydrogel (Fig. 3a and a') is obviously different from that of the hybrid hydrogel (Fig. 3b and b' and c and c'). As shown in Fig. 3a, the pure CMC-*g*-PAA hydrogel displays a relatively smooth and tight surface. However, the hybrid hydrogel containing the GO sheets exhibited an undulant, coarse and rough surface (Fig. 3b and c). Furthermore, with the increase of GO, the rough and super porous structure became more easily identified on the surface and the pores became smaller and more uniform comparing with the pure SAR (Fig. 3c and c'), which will be an added advantage to enhance the water absorbance proficiency of hybrid SARs. This fracture surface morphology change is attributed to the introduction of GO sheets, and then may have some influence on the water permeation regions and swelling behaviors of the corresponding HSARs.

3.3. Swelling behaviors of HSAR

The effect of GO content on swelling ratio of the hybrid hydrogel in distilled water and 0.9 wt% NaCl aqueous solutions was investigated and the results are displayed in Fig. 4. It could be seen that the GO content had an important influence on the water absorbencies of the hybrid SARs. The water absorbencies of the HSARs increased with increasing the content of GO when the content of them is lower than 0.6 wt%. This tendency may be due to the fact that the GO sheets participated in the formation of the three-dimensional network structure, and the introduction of GO sheets greatly decreased the hydrogen bonding interactions among hydrophilic groups and restrained the entanglement of polymer chains, thus the physical crosslinking degree is decreased with the increase of GO. Correspondingly, the swelling capacity enhanced evidently. A similar

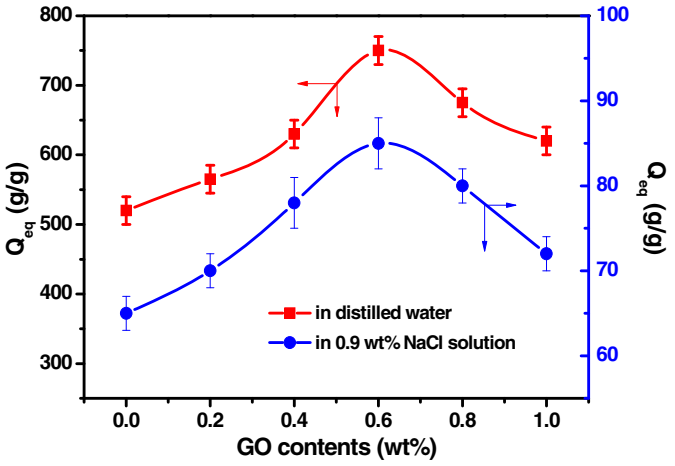

Fig. 4. The effect of GO content on the water absorbency in distilled water and 0.9 wt% NaCl solution. Reaction conditions: AA = 7.2 g, CMC = 12 wt%, MBA = 0.05 wt% and APS = 0.5 wt% at 70 °C.

effect of other inorganic fillers on the SARs has also been reported in the literatures (Ma, Ran et al., 2015; Wang & Wang, 2010). However, with further increasing the GO content from 0.6 to 1.0 wt%, more cross-linking points was generated, which decreases the elasticity of the polymer chains, resulting in the decrease of water absorbency. The highest swelling ratio for the hybrid hydrogel with 0.6 wt% of GO is 750 g g^{-1} in distilled water and 85 g g^{-1} in 0.9 wt% NaCl solution. These results reveal that the incorporation of moderate amount of GO into the CMC-based SAR matrix can enhance the water absorbency. Similar conclusion has also been reported in the petrochemical-based SAR systems, more importantly this CMC-based HSAR showed enhanced performances than previous reported PAA, PAA/GO and PAA-AAm–HNT–GO SARs (Liu, Yu et al., 2013; Zhu et al., 2012). This will provide a novel way to produce low-cost and eco-friendly superabsorbent materials, and render them with great potential for applications in various fields.

Next, the effect of pH on the swelling behaviors of pure CMC-*g*-PAA SAR and CMC-*g*-PAA/GO (0.6 wt% GO) HSAR were investigated in various pH solutions ranging from 2 to 12 (Fig. S4). The solution pH was adjusted by NaOH (pH = 13.0), HCl (pH = 1.0) and distilled water to reach the desired value. It could be seen from Fig. S4, the swelling ratio of the two tested samples showed similar change tendencies towards the change of pH value. When the pH value is less than 5, the swelling ratio of the two tested samples increased drastically with the increase of pH value. When the pH value was increased continually from 5 to 7, the increasing trends of the swelling ratio of the two samples slowed obviously, especially for the pure SAR which reached a relative steady platform with tiny vibration. The maximum value of swelling ratio appeared at pH value 7. When continued to increase the pH from 7 to 12, the swelling ratio of the two tested samples decreased drastically. This result could be explained as follows. When the pH < 5, most of the —COO— group changed into —COOH groups, so the repulsion between polymeric chains decreased, leading to a decrease of water absorbency. When the pH > 10, most of the —COOH groups converted into —COO— groups, and the screening effect of the counter ion (Na^+) on the poly-anionic chain is more evident, which also led to a decrease of the water absorbency. This phenomenon indicated that the buffer action of —COOH and —COO— disappeared when a large amount of acid or base is added. When the pH values kept in the range of 5–10, some of the carboxylate groups were ionized and the ionization degree of the carboxylate groups remains almost constant, which induces a similar osmotic pressure between the hydrogel network and the external solution as well as the electrostatic repulsion among the —COO— groups. In addition, the HSAR

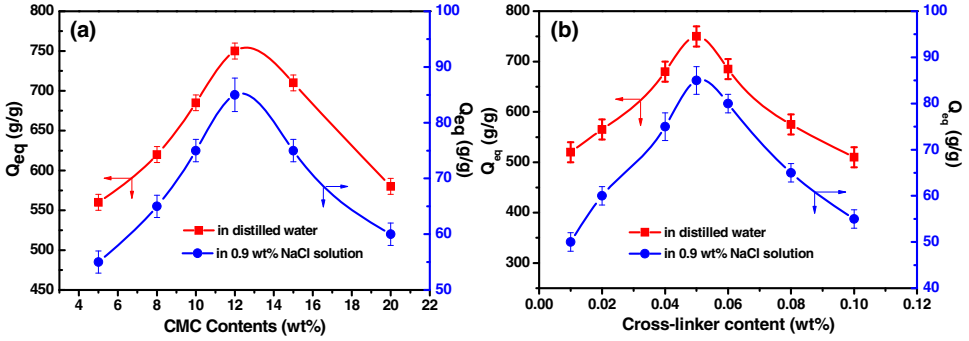

Fig. 5. The effect of (a) CMC content and (b) Cross-linker content on the water absorbency of the HSAR. Reaction conditions: AA = 7.2 g, MBA = 0.05 wt%, APS = 0.5 wt% and GO = 0.5 wt% at 70 °C.

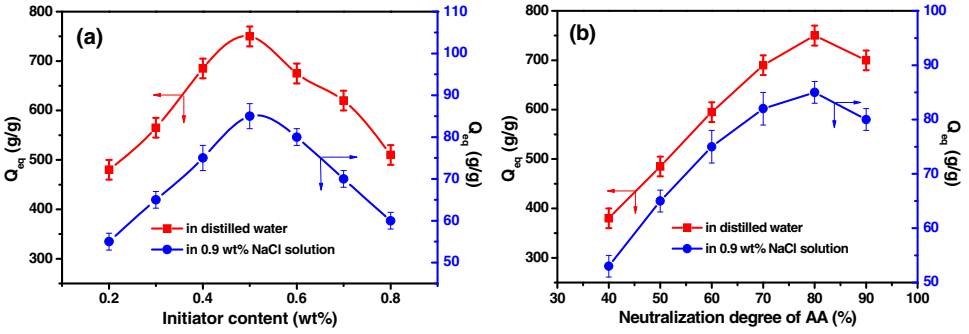

Fig. 6. The effect of (a) initiator content and (b) AA neutralization degree on the water absorbency of HSAR. Reaction conditions: AA = 7.2 g, MBA = 0.05 wt%, CMC = 12 wt% and GO = 0.6 wt% at 70 °C.

showed an enhanced swelling capacity compared with the pure SAR over a wide pH values range of 5–10. The maximum value of swelling ratio also appeared at pH value 7. This phenomenon might result from the incorporation of GO sheets which partially broke the hydrogen bonding interactions among the —COOH groups of the PAA chains, which increased the network size of the hydrogel and thus enhanced the swelling capacity.

The effect of CMC content on water absorbency of CMC-*g*-PAA/GO (0.5 wt% GO) HSAR in distilled water and 0.9 NaCl solution was also examined (Fig. 5a). It could be seen from Fig. 5a that water absorbance of the HSAR increased slightly when the CMC amount was raised from 5 to 12 wt%. This result was possibly resulted from the increase of —OH groups of CMC available to react with AA monomers through graft copolymerization. With the increase of the CMC amount, the homo-polymerization of the AA monomers will decrease in the reaction system, and this can effectively contribute to the increased water absorbency. Nevertheless, when the CMC amount reach 12 wt%, the water absorbency decreased obviously with the continued increase of CMC. This result could be explained as follows. With the increase of CMC, the viscosity of the reaction medium enhanced obviously, which restrained the free movement and uniformly distribution of other reactants in the reaction system. Consequently, both grafting efficiency and the molecular weight of the grafted copolymer chains decreased, which resulted to the decrease of swelling ration. All in all, the CMC amount is a critical factor in preparing high performance natural-based SARs.

The cross-linking density of the hydrogel network in the synthesized composites is a critical swelling control factor and depends upon the amount of cross-linking agent used. In the present study, the variation of MBA amount (0.01–0.10 wt%) was investigated according to water absorbencies of the HSAR with 0.6 wt% GO (Fig. 5b). The water absorbency increased with increasing the content of cross-linking agent from 0.01 to 0.05 wt% and the maximum water absorbency was achieved when the amount of crosslinking agent was 0.05 wt%. This phenomenon is due to the fact that the amount of soluble material increased and the three-dimensional network of the HSAR could not be formed efficiently when the amount of cross-linking agent was lower than 0.05 wt%, which resulted in a smaller swelling ratio of the HSAR. When the amount of cross-linker increased and exceeded 0.05 wt%, more cross-linking points were produced during polymerization and caused the higher cross-linking density and decreased the space of the polymer three-dimensional network. Consequently, it was not beneficial to expand the structure and hold a large quantity of water.

The influence of the initiator content on swelling ratio of CMC-*g*-PAA/GO (0.6 wt% GO) HSAR was investigated by varying the APS concentration in the range of 0.2–0.8 wt% and the results were collected in Fig. 6a. It was evidently seen that the swelling ratio of the HSAR increased considerably with the increase of APS amount in the range of feed ratio from 0.2–0.5 wt% no matter in distilled water or in 0.9 wt% NaCl solution. Thereafter, it started to decrease gradually as the amount of initiator continue to increase. The cause was related to the relationship between average chain length and concentration of the initiator in the polymerization (Zhang, Wang, & Wang, 2007). When the dosage of initiator was low, free radicals on the backbone of cellulose couldn't be fully produced and the polymerization was tardive, which led to less grafted points and grafted monomer amount. More graft polymerization occurred between AA and CMC, leading to the formation of more stable network structures and contributed to the enhancement of water absorbency. When the concentration of the initiator was too high, there was a strong reaction with the cellulose molecular, which resulted in the decrease of the main chain length. Consequently, the water absorbency of the HSAR dropped.

The ratio of available hydrophilic groups such as carboxylic group (—COOH) and carboxyl group (—COO—) in polymeric net-

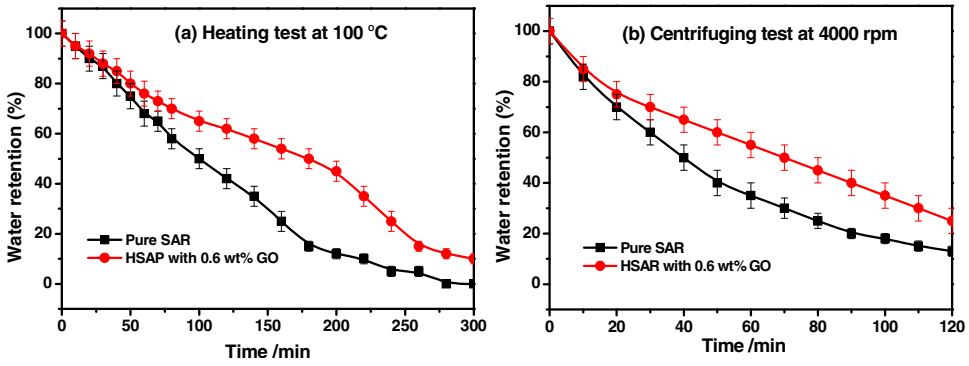

Fig. 7. Water retention behaviors of pure SAR and HSAR with 0.6 wt% GO tested by (a) heating test at 100 °C and (b) centrifuging test at 4000 rpm.

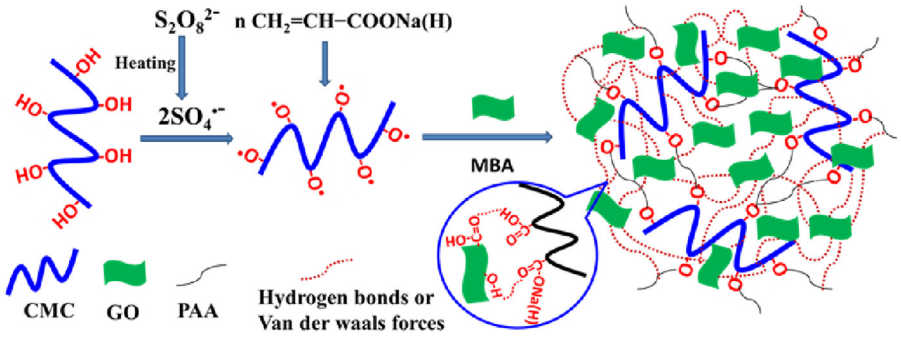

Fig. 8. Schematic illustration of the forming mechanism of the CMC-*g*-PAA/GO HSAR by *in situ* radical co-polymerization.

work have a great influence on the water absorbance of hydrogel. The ratio of these hydrophilic groups can be adjusted by pre-neutralizing the AA monomers. In this study, the AA monomer was partially pre-neutralized with NaOH solution to varied degrees ranging from 40 to 90%. The effect of the neutralization degree of AA on water absorbency of CMC-*g*-PAA/GO (0.6 wt% GO) SAR was assessed and shown in Fig. 6b. It can be seen that the water absorbency increased as the neutralization degree of AA increased, and reached the maximum when the neutralization degree was 80%. Then it decreased with further increase of the neutralization degree of AA. So the optimum neutralization degree was 80%. According to previous studies, the colloid elasticity, ionic osmotic and water affinity have an influence on the swelling ability and absorbencies of hydrogel. The increasing neutralization degree of AA caused more hydrophilic groups on the chain of the composite, thus the network expanded, which was helpful to water absorption. But when the neutralization degree was over 80%, more Na^+ counter ions in the polymeric network would react with the —COO— group and reduce the repulsion, thus resulting in the decrease of water absorbencies. This result is consistent with the literature (Ma et al., 2011).

3.4. Water retention properties of HSAR

Water retention abilities of the CMC-*g*-PAA/GO (0.6 wt% GO) HSAR and pure CMC-*g*-PAA SAR was determined by heating test at 100 °C as well as centrifuging test at 4000 rpm for 10 min each time. As shown in Fig. 7a, both pure SAR and HSAR exhibited a decreasing trend of water retention with pro- longing time. After heating for 80 min at 100 °C, the water retention was found to be 58% for pure SAR and 70% for HSAR, respectively. With prolonging the test time, the HSAR showed a better water-retention ability than that of pure SAR, especially when the duration time ranges from 80 min to 240 min. Similar results were also obtained in the centrifuging test (Fig. 7b). After the centrifuging test for 60 min at 4000 rpm, 58% of water was maintained for HSAR while about 38% of water retention for pure SAR was obtained. Clearly, HSAR obviously showed a better water retention ability than that of pure SAR. According to previous study (Zhu et al., 2012), the water in a hydrogel can be classified into bound water, half-bound water, and free water. Compared to bound water and half-bound water, the free water in a hydrogel has high mobility and can easily be lost. Similar to the structure of layered silicates in a polymer matrix, the irregular dispersion of the GO sheets in the polymeric network of the HSAR may form a so-called “house- of-cards” structure which could serve as a barrier to hinder the diffusion of free water in the network. Therefore, it is suggested that the “barrier effect” of GO sheets would be responsible for the slower release of water from the HSAR than that of pure SAR. Inspired by this observation, this GO hybridized SAR may be attractive in the fields of drug-delivery systems or agriculture applications where the slow release of drugs or fertilizers from hydrogel carriers is essential.

3.5. Forming mechanism of HSAR

Schematically, the proposed mechanism of graft polymerization of partial pre-neutralized AA onto the backbone of CMC in the presence of GO as fillers by using APS as a radical initiator and MBA as a hydrophilic cross-linker was illustrated in Fig. 8. Briefly, sulfate anion radical generated from the hemolytic cleavage of APS initiator, reacts and gives rise to hydroxyl free radical. The sulfate anion radical abstracts hydrogen from the hydroxyl group of the CMC to form alkoxy radicals on the substrate. Then, the resulting radical active centers on the substrate will initiate polymerization of the partial pre-neutralized AA, leading to a graft copolymerization of PAA onto CMC backbone. The copolymer formed in this way

consisted of a cross-linked structure as the MBA was present in the system. Since the GO have rich surface groups, such as —OH and —COOH group, which could participate in the reaction system through hydrogen bonds or Van der Waals forces. Thus, the GO sheets may act as physical cross-linking points in the network and through this process CMC-*g*-PAA/GO HSAR was formed.

4. Conclusion

In summary, an eco-friendly hybrid SAR with well dispersed GO sheets was synthesized through *in situ* copolymerization of partially neutralized AA on CMC backbone in the presence of GO as fillers. It was found that the contents of various factors, such as GO, CMC, cross-linking agent, neutralized degree of AA and initiator had significant influence on the water absorbency and retention behaviors. Under the optimized conditions viz. AA = 7.2 g, neutralization degree = 80%, APS = 0.5 wt%, CMC = 12 wt%, GO = 0.6 wt%, reaction temperature 70 °C, and MBA = 0.05 wt%, the water absorbency of CMC-*g*-PAA/GO HSAR in distilled water and 0.9 wt% NaCl solution were 750 g g^{-1} and 85 g g^{-1}, respectively. According to the results of XRD and SEM, the incorporation of GO sheets had almost no obvious influence on the inherent structure of the SAR but changed the surface morphology markedly. Importantly, the thermal stability, water absorbency and retention ability of the resultant HSAR improved obviously compared to the pure SAR. Moreover, the CMC-*g*-PAA/GO HSAR could retain relatively higher swelling capacity under weak acidic and basic conditions although pH-sensitive swelling behavior. Thus, this kind of hybrid SAR, combining the excellent characteristics of SARs with the unique properties of GO, may find widespread use in a variety of practical applications.

Acknowledgments

Financial support from the key scientific research projects of Henan Province (14B150005 and 17A150028) and the Innovation Research Foundation of Henan Agricultural University is greatly acknowledged.

Appendix A. Supplementary data

Supplementary data associated with this article can be found, in the online version, at http://dx.doi.org/10.1016/j.carbpol.2016.09.070.

References

Bao, Y., Ma, J., & Li, N. (2011). Synthesis and swelling behaviors of sodium carboxymethyl cellulose-*g*-poly(AA-*co*-AM-*co*-AMPS)/MMT superabsorbent hydrogel. *Carbohydrate Polymers*, *84*(1), 76–82. http://dx.doi.org/10.1016/j.carbpol.2010.10.061

Bao, Y., Ma, J., & Sun, Y. (2012). Swelling behaviors of organic/inorganic composites based on various cellulose derivatives and inorganic particles. *Carbohydrate Polymers*, *88*(2), 589–595. http://dx.doi.org/10.1016/j.carbpol.2012.01.003

Chen, J., Zhang, W., & Li, X. (2015). Preparation and characterization of a novel superabsorbent of konjac glucomannan-poly(acrylic acid) with trimethylolpropane trimethacrylate cross-linker. *RSC Advances*, *5*(48), 38417–38423. http://dx.doi.org/10.1039/C5RA04522C

Compton, O. C., & Nguyen, S. T. (2010). Graphene oxide, highly reduced graphene oxide, and graphene: Versatile building blocks for carbon-based materials. *Small*, *6*(6), 711–723. http://dx.doi.org/10.1002/smll.200901934

Dreyer, D. R., Park, S., Bielawski, C. W., & Ruoff, R. S. (2010). The chemistry of graphene oxide. *Chemical Society Reviews*, *39*(1), 228–240. http://dx.doi.org/10.1039/B917103G

Ferfera-Harrar, H., Aiouaz, N., Dairi, N., & Hadj-Hamou, A. S. (2014). Preparation of chitosan-*g*-poly(acrylamide)/montmorillonite superabsorbent polymer composites: Studies on swelling, thermal, and antibacterial properties. *Journal of Applied Polymer Science*, *131*(1), 39747. http://dx.doi.org/10.1002/app.39747

Huang, Y., Lu, J., & Xiao, C. (2007). Thermal and mechanical properties of cationic guar gum/poly(acrylic acid) hydrogel membranes. *Polymer Degradation and Stability*, *92*(6), 1072–1081. http://dx.doi.org/10.1016/j.polymdegradstab.2007.02.011

Huang, Y., Zeng, M., Ren, J., Wang, J., Fan, L., & Xu, Q. (2012). Preparation and swelling properties of graphene oxide/poly(acrylic acid-*co*-acrylamide) super-absorbent hydrogel nanocomposites. *Colloids and Surfaces A: Physicochemical and Engineering Aspects*, *401*, 97–106. http://dx.doi.org/10.1016/j.colsurfa.2012.03.031

Huang, Z., Liu, S., Fang, G., & Zhang, B. (2013). Synthesis and swelling properties of β-cyclodextrin-based superabsorbent resin with network structure. *Carbohydrate Polymers*, *92*(2), 2314–2320. http://dx.doi.org/10.1016/j.carbpol.2012.12.002

Huang, Y., Zeng, M., Feng, Z., Yin, D., Xu, Q., & Fan, L. (2016). Graphene oxide-based composite hydrogels with self-assembled macroporous structures. *RSC Advances*, *6*(5), 3561–3570. http://dx.doi.org/10.1039/C5RA25910J

Hummers, W. S., & Offeman, R. E. (1958). Preparation of graphitic oxide. *Journal of the American Chemical Society*, *80*, 1939. Retrieved from. http://pubs.acs.org/doi/pdf/10.1021/ja01539a017

Irani, M., Ismail, H., & Ahmad, Z. (2014). Hydrogel composites based on linear low-density polyethylene-*g*-poly (acrylic acid)/Kaolin or halloysite nanotubes. *Journal of Applied Polymer Science*, *131*(8), 40101. http://dx.doi.org/10.1002/app.40101

Kovtyukhova, N. I., Ollivier, P. J., Martin, B. R., Mallouk, T. E., Chizhik, S. A., Buzaneva, E. V., & Gorchinskiy, A. D. (1999). Layer-by-layer assembly of ultrathin composite films from micron-sized graphite oxide sheets and polycations. *Chemistry of Materials*, *11*(3), 771–778. http://dx.doi.org/10.1021/cm981085u

Liu, J., Chu, H., Wei, H., Zhu, H., Wang, G., Zhu, J., & He, J. (2016). Facile fabrication of carboxymethyl cellulose sodium/graphene oxide hydrogel microparticles for water purification. *RSC Advances*, *6*(55), 50061–50069. http://dx.doi.org/10.1039/C6RA06438H

Liu, J., Li, Q., Su, Y., Yue, Q., Gao, B., & Wang, R. (2013). Synthesis of wheat straw cellulose-*g*-poly (potassium acrylate)/PVA semi-IPNs superabsorbent resin. *Carbohydrate Polymers*, *94*(1), 539–546. http://dx.doi.org/10.1016/j.carbpol.2013.01.089

Liu, C., Yu, L., Zhang, Y., Zhang, B., Liu, J., & Zhang, H. (2013). Preparation of poly(sodium acrylate-acrylamide) superabsorbent nanocomposites incorporating graphene oxide and halloysite nanotubes. *RSC Advances*, *3*(33), 13756–13763. http://dx.doi.org/10.1039/c3ra23094e

Ma, Z., Li, Q., Yue, Q., Gao, B., Xu, X., & Zhong, Q. (2011). Synthesis and characterization of a novel super-absorbent based on wheat straw. *Bioresource Technology*, *102*(3), 2853–2858. http://dx.doi.org/10.1016/j.biortech.2010.10.072

Ma, J., Li, X., & Bao, Y. (2015). Advances in cellulose-based superabsorbent hydrogels. *RSC Advances*, *5*(73), 59745–59757. http://dx.doi.org/10.1039/C5RA08522E

Ma, G., Ran, F., Yang, Q., Feng, E., & Lei, Z. (2015). Eco-friendly superabsorbent composite based on sodium alginate and organo-loess with high swelling properties. *RSC Advances*, *5*(66), 53819–53828. http://dx.doi.org/10.1155/2014/675035

Morimune, S., Nishino, T., & Goto, T. (2012). Poly(vinyl alcohol)/graphene oxide nanocomposites prepared by a simple eco-process. *Polymer Journal*, *44*(10), 1056–1063. http://dx.doi.org/10.1038/pj.2012.58

Muhammad, G., Hussain, M. A., Ashraf, M. U., Haseeb, M. T., Hussain, S. Z., & Hussain, I. (2016). Polysaccharide based superabsorbent hydrogel from Mimosa pudica: Swelling–deswelling and drug release. *RSC Advances*, *6*(28), 23310–23317. http://dx.doi.org/10.1039/C5RA23088H

Mukerabigwi, J. F., Lei, S., Wang, H., Luo, S., Ma, X., Qin, J., . . . & Cao, Y. (2015). Synthesis and properties of a novel ecofriendly superabsorbent hydrogel nanocomposite based on xyloglucan-graft-poly(acrylic acid)/diatomite. *RSC Advances*, *5*(102), 83732–83742. http://dx.doi.org/10.1039/C5RA12355K

Mukerabigwi, J. F., Lei, S., Fan, L., Wang, H., Luo, S., Ma, X., . . . & Cao, Y. (2016). Eco-friendly nano-hybrid superabsorbent composite from hydroxyethyl cellulose and diatomite. *RSC Advances*, *6*(38), 31607–31618. http://dx.doi.org/10.1039/C6RA01759B

Novoselov, K. S., Geim, A. K., Morozov, S. V., Jiang, D., Zhang, Y., Dubonos, S. V., . . . & Firsov, A. A. (2004). Electric field effect in atomically thin carbon films. *Science*, *306*(5696), 666–669. http://dx.doi.org/10.1126/science.1102896

Peng, N., Wang, Y., Ye, Q., Liang, L., An, Y., Li, Q., & Chang, C. (2016). Biocompatible cellulose-based superabsorbent hydrogels with antimicrobial activity. *Carbohydrate Polymers*, *137*, 59–64. http://dx.doi.org/10.1016/j.carbpol.2015.10.057

Tripathi, A. M., & Mitra, S. (2016). Solvent transfer of graphene oxide for synthesis of tin mono-sulfide graphene composite and application as anode of lithium-ion battery. *Materials Science and Engineering: B*, http://dx.doi.org/10.1016/j.mseb.2016.03.006

Wang, Z., & Chen, Y. (2007). Supramolecular hydrogels hybridized with single-walled carbon nanotubes. *Macromolecules*, *40*(9), 3402–3407. http://dx.doi.org/10.1021/ma0702593

Wang, W., & Wang, A. (2010). Nanocomposite of carboxymethyl cellulose and attapulgite as a novel pH-sensitive superabsorbent: Synthesis, characterization and properties. *Carbohydrate Polymers*, *82*(1), 83–91. http://dx.doi.org/10.1016/j.carbpol.2010.04.026

Wang, Z., Xu, C., Gao, G., & Li, X. (2014). Facile synthesis of well-dispersed Pd–graphene nanohybrids and their catalytic properties in 4-nitrophenol reduction. *RSC Advances*, *4*(26), 13644–13651. http://dx.doi.org/10.1039/c3ra47721e

Wilson, N. R., Pandey, P., Beanland, R., Young, R. J., Kinloch, I., Gong, L., . . . & Sloan, J. (2009). Graphene oxide: Structural analysis and application as a highly

transparent support for electron microscopy. *ACS Nano*, *3*(9), 2547–2556. http://dx.doi.org/10.1021/nn900694t

Zhang, J., Wang, Q., & Wang, A. (2007). Synthesis and characterization of chitosan-*g*-poly(acrylic acid)/attapulgite superabsorbent composites. *Carbohydrate Polymers*, *68*(2), 367–374. http://dx.doi.org/10.1016/j.carbpol.2006.11.018

Zhang, H., Zhai, D., & He, Y. (2014). Graphene oxide/polyacrylamide/carboxymethyl cellulose sodium nanocomposite hydrogel with enhanced mechanical strength: Preparation, characterization and the swelling behavior. *RSC Advances*, *4*(84), 44600–44609. http://dx.doi.org/10.1039/C4RA07576E

Zhu, Z.-Q., Sun, H.-X., Qin, X.-J., Jiang, L., Pei, C.-J., Wang, L., . . . & Deng, W.-Q. (2012). Preparation of poly(acrylic acid)–graphite oxide superabsorbent nanocomposites. *Journal of Materials Chemistry*, *22*(11), 4811–4817. http://dx.doi.org/10.1039/c2jm14210d